ELSEVIER

Microporous and Mesoporous Materials 22 (1998) 165–178

MICROPOROUS AND MESOPOROUS MATERIALS

Spectroscopy and coordination chemistry of cobalt in molecular sieves[1]

An A. Verberckmoes *, Bert M. Weckhuysen, Robert A. Schoonheydt

Centrum voor Oppervlaktechemie en Katalyse, Departement Interfasechemie, K.U. Leuven, Kardinaal Mercierlaan 92, 3001 Heverlee (Leuven), Belgium

Received 17 December 1997; received in revised form 15 February 1998; accepted 18 February 1998

Abstract

The catalytic potential of Co-containing molecular sieves has stimulated zeolite scientists to study the spectroscopy and siting of Co^{2+} ions. In this review, a critical overview is given of the spectroscopic tools used: (1) to decide about the cation sites of Co^{2+} and their occupancy; (2) to determine the spectroscopic signatures of framework and extra-framework cobalt; (3) to determine the amount of Co incorporated into the framework of molecular sieves; and (4) to discuss local distortions of framework cobalt. © 1998 Elsevier Science B.V. All rights reserved.

Keywords: Cobalt; Molecular sieves; DRS; EPR; XAS; XPS

1. Introduction

Transition metal ion-containing molecular sieves are extensively investigated in academic and industrial laboratories because of their promising catalytic behaviour in the oxidation of organic compounds [1–5] and in the removal of NO_x [6–18]. In this respect, cobalt is an interesting transition metal ion, not only because of its promising catalytic activity, but also because of the rich spectroscopy of its divalent state.

Co^{2+} can be introduced into molecular sieves in two different ways: (1) ion exchange [19,20], including solid state ion exchange; and (2) hydrothermal synthesis. In the first case, Co^{2+} occupies different exchange sites in order to minimize the energy of the unit cell. In the second case, both lattice and extra-lattice Co^{2+} may be found. In any case, the result is Co^{2+} in different coordination geometries, often occurring simultaneously. Spectroscopy only gives an overall picture. If one wants detailed information on siting at the surface or in the lattice, spectroscopic signatures of each Co^{2+} site must be extracted from the overall spectra and interpreted in terms of local geometries. Thus, spectroscopy typically gives local information; i.e. about the first coordination sphere. X-ray diffraction gives average information on occupancy and coordination distances.

2. Spectroscopic tools for Co^{2+} siting

With the exception of some zeolite-encaged low-spin Co^{2+} complexes (e.g. Schiff base complexes

* Corresponding author. Fax: +32 16 32 1998;
E-mail: an.verberckmoes@agr.kuleuven.ac.be

[1]Dedicated to Professor Lovat V.C. Rees in recognition and appreciation of his lifelong devotion to zeolite science and his outstanding achievements in this field.

PII: S1387-1811(98)00091-2

[21]), Co^{2+} ions (d^7) are always present in their high-spin state. Thus, the oxygen atoms in zeolites can be regarded as weak ligands [22]. Useful spectroscopic techniques must then be capable of discriminating between the different coordinations of high-spin Co^{2+}. Because of the complex and overlapping spectra, band decomposition and chemometrical tools are needed, especially if quantitative information is desired. Below, the fundamentals of the techniques are given in order to understand the spectroscopic signatures of Co^{2+}, coordinated to structural oxygen atoms.

2.1. Diffuse reflectance spectroscopy

Diffuse reflectance spectroscopy (DRS) [23–25] detects the d–d transitions of Co^{2+} in the near infrared and visible region, and the $O \rightarrow Co^{2+}$ charge transfer transitions in the ultraviolet region. Two representative cases, high-spin octahedral and tetrahedral Co^{2+}, will be discussed [26–33]. The ligand field energy-level diagram is given in Fig. 1. Δ_T and Δ_O represent the tetrahedral and octahedral ligand field splitting parameter $10Dq$, respectively. Octahedral complexes exhibit three transitions from their ground state $^4T_{1g}(F)(t_{2g}^5 e_g^2)$: $\nu_1 \equiv {}^4T_{1g}(F) \rightarrow {}^4T_{2g}(F)$; $\nu_2 \equiv {}^4T_{1g}(F) \rightarrow {}^4A_{2g}(F)$; $\nu_3 \equiv {}^4T_{1g}(F) \rightarrow {}^4T_{1g}(P)$, and $\nu_1 - \nu_2$ equals $10Dq$, the ligand field splitting parameter. All d–d transitions in octahedral complexes are symmetry forbidden.

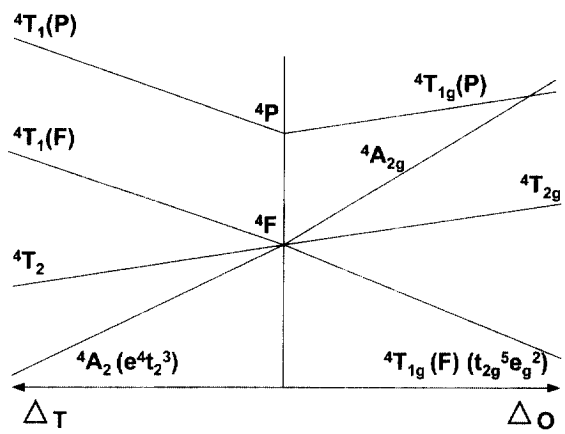

Fig. 1. Energy-level diagram of Co^{2+} in a tetrahedral and octahedral ligand field.

This can be generalized to all complexes with a symmetry centre.

Tetrahedral complexes also exhibit three transitions from the ground state $^4A_2(F)(e^4t_2^3)$: $\nu_1 \equiv {}^4A_2(F) \rightarrow {}^4T_2(F)$; $\nu_2 \equiv {}^4A_2(F) \rightarrow {}^4T_1(F)$; $\nu_3 \equiv {}^4A_2(F) \rightarrow {}^4T_1(P)$. All the transitions are symmetry and spin allowed; i.e. there is no symmetry centre and $\Delta S = 0$. However, ν_1 always lies in the infrared (IR) region; i.e. between 2500 and 6000 cm^{-1}, whereas the ν_2 and ν_3 transitions are often split into three components and are found respectively in the NIR and visible region. The band splitting may be due to (i) a low symmetry perturbation which lifts the degeneracy of the two $^4T_1$ excited levels, (ii) a dynamic Jahn–Teller effect which splits the two bands into three symmetrically spaced peaks, or (iii) spin–orbit coupling. The visible region of both octahedral and tetrahedral Co^{2+} complexes is dominated by the highest energy transition ν_3, $^4A_2 \rightarrow {}^4T_1(P)$ around 16 000–17 000 cm^{-1} for tetrahedral, and $^4T_{1g}(F) \rightarrow {}^4T_{1g}(P)$ around 20 000 cm^{-1} for octahedral complexes. Furthermore, the latter transition is around two orders of magnitude less intense than the tetrahedral one.

Complexes with a symmetry centre can gain intensity through vibronic coupling; i.e. coupling between the electronic states and normal modes of vibration of appropriate symmetry. Similarly, spin forbidden transitions may become partially allowed by spin–orbit coupling, connecting states with $\Delta S \pm 1$.

2.2. Electron paramagnetic resonance

Electron paramagnetic resonance (EPR) [34–37] is a very sensitive technique to study the coordination of high-spin Co^{2+}, but spin–lattice relaxation often precludes the observation of EPR signals, especially those from octahedral Co^{2+}. In the case of (distorted) tetrahedral Co^{2+} ($S = 3/2$), typical g-values around 1.77, 2.62 and 5.82 are observed below 77 K. The ligand field energy-level diagram of the ground state $^4A_2$ is given in Fig. 2. Distortion of the tetrahedron will split the $^4A_2$ ground state into two Kramer's doublets ($m_s = \pm 1/2$ and $\pm 3/2$), which are degenerated in the absence of a magnetic field H. This is called

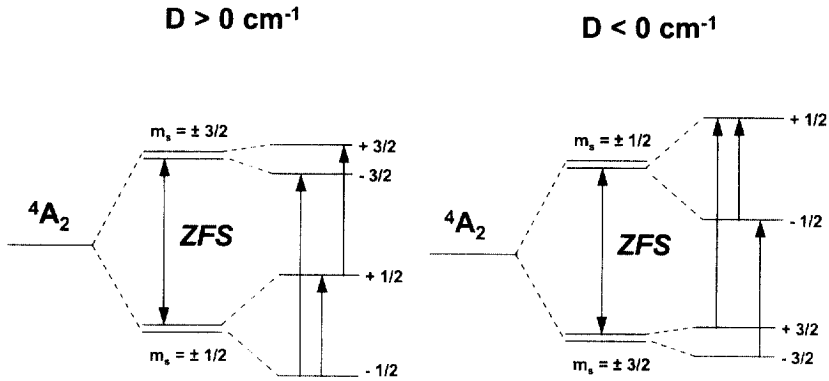

Fig. 2. Overview of the possible EPR transitions for tetrahedral Co^{2+}.

the zero field splitting (ZFS), and the corresponding energy splitting between the two doublets is given by $2(D^2+3E^2)^{1/2}$, with D and E the zero field splitting parameters. In the case of axial distortions ($E=0$), the energy difference between the two doublets equals $2D$. The sign of the ZFS; i.e. $2D$, is determined by whether the $m_s=\pm 1/2$ or $m_s=\pm 3/2$ doublet lies lowest. By convention, the value of D is positive when $m_s=\pm 1/2$ is lowest and negative when $m_s=\pm 3/2$ is lowest. Tetrahedral D values are usually between -10 and $10\,cm^{-1}$. In the presence of a magnetic field H, the two degenerate doublets $m_s=\pm 1/2$ and $\pm 3/2$ are split up, and an incident microwave will induce transitions according to the selection rule $\Delta m_s=\pm 1$. The three possible transitions, giving rise to an EPR signal, are included in Fig. 2.

High-spin Co^{3+} in (distorted) tetrahedral coordination (d^6; $S=2$) is only EPR visible at low temperature. In Fig. 3, the ligand field energy-level diagram of the ground state ^5E is shown. The energy splittings are due to symmetry distortion (ZFS), and the presence of a magnetic field H. However, due to the close proximity of the electronic excited state $^5T_2$, very low temperatures are needed to see the transitions from the non-degenerate $m_s=0$ spin state to the higher lying ± 1 doublet.

2.3. X-ray absorption spectroscopy

X-ray absorption spectroscopy (XAS) is a spectroscopic technique, in which an electron is excited

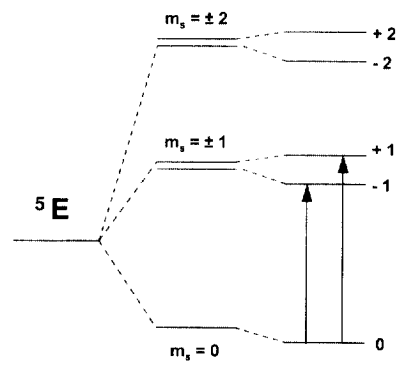

Fig. 3. Overview of the possible EPR transitions for tetrahedral Co^{3+}.

from one energy level to another and the ejected electron is scattered from atoms surrounding the absorbing atom [38]. Contributions to the XAS signal dominantly result from the other two or three closest shells of atomic neighbours surrounding the absorbing atom, and consequently it is a local structure probe. XAS determines pre-, near- and extended-edge structures, and is therefore commonly subdivided into pre-edge X-ray absorption (PEXA), X-ray absorption near-edge structures (XANES) and extended X-ray absorption fine structure (EXAFS) [39]. The XAS spectrum is generated by exposing a sample to an incident monochromatic beam of synchrotron X-rays in the range 0.5 to 100 keV. When the energy of the incident X-ray beam ($h\nu$) is less than the binding energy (E_b) of a core electron of the element of interest, little absorption takes place. However,

when $hv \approx E_b$, electronic transitions to unoccupied bound energy levels occur, contributing to the main absorption edge and producing features below the main edge, referred to as the pre-edge spectrum. As hv increases beyond E_b, electrons can be ejected to continuum; i.e. unbound levels, and remain in the vicinity of the absorber for a short time with excess kinetic energy. In the energy region extending from just above to about 50 eV above E_b, the electrons are multiply scattered among neighbouring atoms, which produces the XANES spectrum. When hv is about 50 to 1000 eV above E_b, electrons are ejected from the absorber, and then leave the vicinity of the absorber. The EXAFS spectrum is due to interferences between outgoing and backscattered photoelectrons, which modulates the atomic absorption coefficient. The pre-, near- and extended-edge structures provide extremely detailed information on the local structure of Co and on the number and distance of neighbouring atoms. However, it is important to notice that the obtained information is only an average of possible coordination environments. As a consequence, data handling and interpretation is not easy, and requires long-standing expertise.

The Co K-edge XANES spectra of as-synthesized Co-substituted molecular sieves have the pre-edge feature (denoted as the 1s→3d transition) around 7710 eV, which is typical for Co^{2+} in tetrahedral coordination [40]. From the Co K-edge EXAFS, together with the associated Fourier transforms, the coordination distance of the first shell can be deduced. For different types of CoAPO-*n* materials, the degree of oxidation has been estimated from the extent of the decrease in the Co–O distance. Also, a shift of the K-edge position after calcination was observed. Comparison between the X-ray absorption edge-position of Co^{2+} and Co^{3+} in oxides and cobaloximes suggest that the shift is of the order of 1.5–3 eV [41,42]. An example of an EXAFS study, where Co^{2+} ions are not in a tetrahedral lattice position but form finely dispersed Co oxide clusters, is reported for Co/MCM-41 [43].

2.4. X-ray photoelectron spectroscopy

X-ray photoelectron spectroscopy (XPS) or electron spectroscopy for chemical analysis (ESCA) [44,45] is based on the irradiation of a sample in ultra-high vacuum by monoenergetic soft X-rays [usually Mg Kα (1253.6 eV) or Al Kα (1486.6 eV)] and analysing the energy of the detected electrons. The spectrum is obtained by plotting the number of detected electrons per energy interval versus their kinetic energy. Because the mean free path of electrons in solids is very small, the detected electrons originate from only the top few atomic layers, making XPS a surface-sensitive technique for chemical analysis. The interact of the photons with atoms in the surface region causes electrons to be emitted by the photo-electric effect. The emitted electrons have measured kinetic energies given by:

$$KE = hv - BE - \phi_s$$

where hv is the energy of the photon, BE is the binding energy of the atomic orbital from which the electron originates, and ϕ_s is the spectrometer work function.

Quantitative data of the XPS measurements can be obtained from peak heights or peak areas, and identification of chemical states can often be made from exact measurement of peak positions and separations, as well as from certain spectral features. In comparison with other spectroscopic techniques, XPS is not so sensitive.

In the case of cobalt, the 2p transitions are measured. Upon ionization, the 2p level becomes split into $2p_{1/2}$ and $2p_{3/2}$. The spin–orbit coupling ratio for the 2p level is 1:2. Co^{2+} in oxidic materials or ion-exchanged in zeolites, e.g. in Co-ZSM-5 [46,47], is characterized by a $2p_{3/2}$ peak around 782 eV with an intense shoulder at 787–788 eV. The $2p_{1/2}$ peak is separated by about 15.7 eV at higher energy. When, upon calcination, Co^{3+} is formed at the expense of the amount of Co^{2+}, the main $2p_{3/2}$ peak shifts to lower energy and its shoulder decreases in intensity. Formation of Co_3O_4 crystallites is visible in XPS by a $2p_{3/2}$ peak at 781 eV, and complete reduction to cobalt metal is characterized by a peak at 778 eV [46,47].

3. Cobalt at cation exchange sites

Co^{2+} ions are usually exchanged as hexa–aquo complexes in the supercages and channels of

molecular sieves. To avoid side reactions such as proton exchange and precipitation of hydroxides, the exchange must be performed in a dilute, neutral to slightly acidic solution [48]. Heating in air or oxygen results in a release of water molecules. In addition, the Co^{2+} ions migrate towards the smaller cavities, where they occupy well-defined cation sites. This is the case for zeolites A, X and Y, and in most of the low-silica zeolites. Instead, for high-silica zeolites, the cation sites are much less defined or even not yet known. Therefore, Co^{2+} siting will be much more difficult. Many studies have been done on Co-ZSM-5 because of its effectiveness in the selective catalytic reduction of NO by hydrocarbons, e.g. TPD and IR studies of NO adsorbed on Co-ZSM-5 [49–51], but the main purpose of these studies was to identify the reaction mechanism [9,16,18,52], rather than to elucidate the Co^{2+} siting itself.

Although X-ray diffraction (XRD) [53] is a powerful tool for Co^{2+} siting, only a limited number of results for CoA and CoY are reported in the literature. In dehydrated zeolite A, Co^{2+} ions occupy the plane of the six-ring (site I). In zeolite Y after dehydration, at least two sites are occupied, sites I and I′, but site I in the hexagonal prism is the favoured one. For CoMOR, no XRD results are available, but a comparison can be made with the siting of Ca^{2+} in mordenite [53,54].

It is also clear that the X-ray diffraction technique has some limitations because: (1) only average bond distances and average coordination numbers of Co^{2+} at a certain cation site can be obtained; (2) no distinction can be made between Si and Al atoms; and (3) high cobalt loadings are always necessary. In this respect, spectroscopic measurements have some advantages because small Co loadings are required to obtain well-resolved spectra. This is certainly the case for EPR.

3.1. Diffuse reflectance spectroscopy

Fig. 4 shows the spectra of CoNaY upon dehydration. In the hydrated, pink sample (curve 1), spectral maxima appear around 20 000 cm^{-1} (500 nm) in the VIS region and at 8000 cm^{-1} in the NIR. These absorptions are assigned to ν_3 and ν_1 transitions of the octahedral $[Co(H_2O)_6]^{2+}$ complex in the supercages [22,55]. The sharp bands at 7000 cm^{-1} and 5200 cm^{-1} originate from overtone and combination bands of adsorbed H_2O. After dehydration at 100°C, the sample turns purple and the spectral intensity increases. After dehydration at 150°C, the sample is blue and two ranges of absorption have developed, one in the 16 000–19 000 cm^{-1} region and one in the 5000–9000 cm^{-1} region. Both are split into three components. These triplets are due to $\nu_2 \equiv {}^4A_2(F) \rightarrow {}^4T_1(F)$ and $\nu_3 \equiv {}^4A_2(F) \rightarrow {}^4T_1(P)$ transitions. Co^{2+} is located at sites I′, II′ or II, where it is coordinated to three oxygens of the sodalite six-rings and to a fourth ligand, which is determined by IR to be H_2O [55]. Further dehydration intensifies the spectrum and at 200°C the band at 16 000 cm^{-1} has shifted to 15 250 cm^{-1}. At higher temperature, the intensity decreases and at 470°C a band at 13 700 cm^{-1} is clearly apparent.

The shift from a symmetrical triplet at 150°C to an asymmetrical triplet at 200°C has been explained either by a change in ligand (H_2O or OH or O^{2-}) [56–62] or as a distortion of the tetrahedron [55]. For the $Co(O)_3OH$ complex, IR spectra show that the OH groups are not stable if bonded to cations at 350°C and easily dehydroxylate [55]. The decrease in intensity with increasing dehydration temperature points towards the migration of Co^{2+} in faujasite from a tetrahedral species in the sodalite cage to an octahedral species in the hexagonal prism [55,59,63] and is confirmed by XRD data [53]. Sometimes a band at 25 000 cm^{-1} can be observed. Pure oxide (CoO) and many mixed oxides of Co^{2+} exhibit an absorption in the 25 000–27 000 cm^{-1} region [64], but because a similar band is present in CoNaA, it can also be attributed to trigonal coordination of Co^{2+} [63]. The band at 13 800 cm^{-1} in CoNaY has been assigned to Co^{2+} at site I, having octahedral symmetry [55,63].

The spectrum of calcined CoNaA has triplet bands at 18 600, 17 250 and 15 700 cm^{-1}; the latter band having the highest intensity. CoNaA also has a band at 13 700 cm^{-1} as in the CoNaY spectrum. For CoNaA often a three-fold coordination has been proposed [58,59]. Klier was the first to

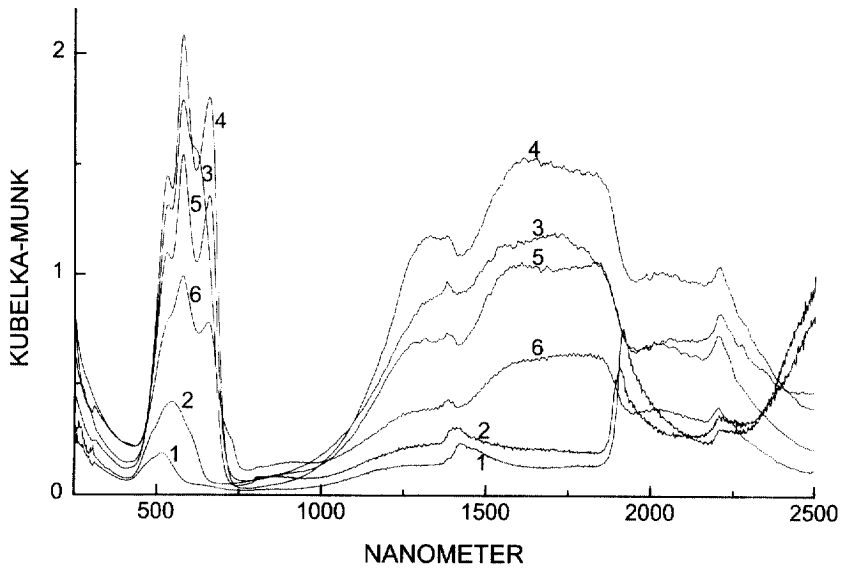

Fig. 4. Diffuse reflectance spectrum of CoNaY upon dehydration: (1) hydrated; (2) 100°C (3 h); (3) 150°C (3 h); (4) 200°C (3 h); (5) 300°C; (6) 470°C (8 h).

interpret the CoA spectrum with ligand field theory in a D_{3h} configuration [65,66].

3.2. Electron paramagnetic resonance

Heilbron and Vickerman performed combined DRS–EPR measurements for CoA, CoX and CoY zeolites (all in the Na^+ form) during the dehydration process up to 600°C [60]. The data at the highest dehydration temperatures are given in Table 1. They interpreted the DRS and EPR results as follows: at 400°C and 600°C a $Co(Ox)_3OH^-$ or $Co(Ox)_3O^{2-}$ species (Ox = lattice oxygen) is formed at the six-ring site in A (and no three-fold coordination as found with XRD [58]). The same species can be formed in CoX and CoY at 400°C at the six-ring sites I′ and II′. At 600°C, a $Co(Ox)_3O^{2-}$ species is formed at sites I′ or II′ and a $Co(Ox)_6$ species is found in the hexagonal prism (site I). The $g_\perp = 5.5$ and $g_\parallel = 2.05$ of CoA (400°C) are attributed to Co^{2+} in an elongated tetrahedral environment. The other EPR parameters ($g_\parallel \sim 3.3$, $g_\perp \sim 2.1$, $g_{average} = 2.2$) are attributed to a compressed tetrahedral environment. Such an environment would be expected to give a negative zero field splitting parameter (D). If this parameter

Table 1
DRS and EPR data of Co^{2+}-exchanged zeolites and of CoAPO-5

	DRS ($\times 10^3$ cm^{-1})						EPR	Temperature behaviour	Reference
CoA (400°C)		15.7	16.8	19.5	24		(i) $g_\perp = 5.5$, $g_\parallel = 2.05$ (ii) $g \sim 3.3$, $g \sim 2.1$		[60]
CoA (600°C)		14.8	16.8	19.5	26		$g_\parallel \sim 3.3$, $g_\perp \sim 2.1$, $g_{av} = 2.2$	Temp. ↓, Int. ↓	[60]
CoX, Y (400°C)	13.5	15.0	17.1	18.9			$g_{av} = 2.2$, for $X \sim 2.1$	Temp. ↓, Int. ↓	[60]
CoY (600°C)	13.5	15.4	17.1	18.9	21		$g_\parallel \sim 3.3$, $g_\perp \sim 2.1$, $g_{av} = 2.2$	Temp. ↓, Int. ↓	[60]
CoX (600°C)	13.8	14.6		19.8			$g_\perp \sim 36$, $g_\parallel \sim 2$	Temp. ↓, Int. ↑	[60]
CoAPO-5 synth.		16	17.3	18.5			$g_\perp = 6.15$, $g_\parallel = 2.23$	Temp. ↓, Int. ↑	[88]
CoAPO-5 calc.		15.5	17.3	(19.5)	25.2	31.5	$g_\perp = 5.35$, $g_\parallel = 2.34$	Temp. ↓, Int. ↓	[88]

is large ($\sim -10\ cm^{-1}$) a transition within the $\pm 1/2$ doublet would only be expected to appear when its population becomes appreciable, hence the apparent increase of intensity with increasing temperature. The EPR signal of CoX (600°C) is assigned to octahedral Co^{2+} at site I. Its signal is only observable below 100 K.

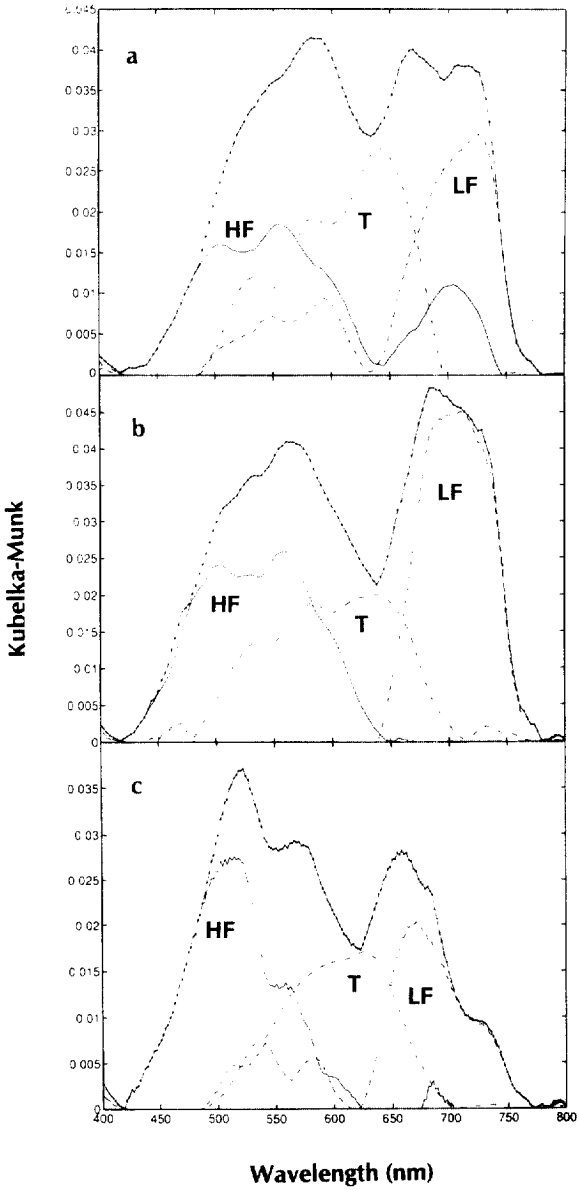

Fig. 5. The global spectrum and resolved pure components of the data series of (a) CoY dehydrated at 400°C, (b) CoY dehydrated at 500°C, and (c) CoX dehydrated at 400°C. The symbols T, LF and HF represent the triplet component, low-frequency component and high-frequency component, respectively (reprinted from ref. [73], copyright American Chemical Society, 1995).

3.3. Chemometrical approach

Till now, spectral changes have been interpreted in the general scheme $Co(H_2O)_6^{2+} \rightarrow Co(Ox)_3(H_2O) \rightarrow Co(Ox)_3(OH^-)$, $Co(Ox)_3(O^{2-})$ $Co(Ox)_3 \rightarrow$(except for zeolite A) $Co(Ox)_6$, but the full spectroscopic signatures of each of these species are not yet known, because they give strongly overlapping spectra. In order to unravel such overlapping spectra, chemometrical techniques, such as principal component analysis (PCA) [67–69] and an interactive self-modeling analysis (SIMPLISMA) [70–72], have been used. Series of dehydrated CoNaA, CoNaX and CoNaY zeolites, all differing in only one parameter, the Co^{2+} loading, have been analysed by these methods [73–75]. Two components were determined for CoA: trigonal and pseudo-tetrahedral Co^{2+} at the six-ring site, and three components for CoX and CoY: pseudo-octahedral Co^{2+} in the hexagonal prism, and pseudo-tetrahedral and trigonal Co^{2+} at site I′. As an example, the pure spectra of CoY and CoX are given in Fig. 5. The positions of the pure components are given in Table 2.

Because of the unique correspondence for CoY between the decomposed bands with a deconvolution program, and the components obtained with SIMPLISMA, both in position and intensity course, the quantitative information on the decomposed DRS spectra was used to predict the preferred positions of Co^{2+} [73]. By means of XRD results of dehydrated $Co_{14}Y$ at 500°C, with a distribution of 11.3 Co^{2+} at site I and 2.3 Co at site I′ [76], the molar extinction coefficient of Co^{2+} at I′/I was determined to be 26.8, and the distribution of Co^{2+} at all loadings could be observed as shown in Table 3. It is found that for all loadings around 80% of Co^{2+} is at site I. These studies are only performed at room temperature. Cations do move around in molecular sieves and site populations can change. In situ studies would be useful to investigate the cations at higher temperatures and in different atmospheres to assess the coordination of these cations under catalytic conditions.

Table 2
Frequencies (cm^{-1}) of the pure components of dehydrated CoY, CoX and CoA zeolites, obtained with SIMPLISMA [73,74]

CoY	CoX	CoA
	Component 1: trigonal Co^{2+}	
14000	(13700)–14900	13550–15750–17200–18300
	Component 2: pseudo-tetrahedral Co^{2+}	
15650–17150–18700	15950–17000	15000–16200–19550
	Component 3: pseudo-octahedral Co^{2+}	
17850–20000	17850–19600	/

Table 3
Co^{2+} distribution along pseudo-octahedral and pseudo-tetrahedral/trigonal sites at all loadings, calculated with the band areas and with a molar extinction coefficient of Co^{2+} at I'/I of 26.8

		Adjusted Kubelka–Munk band areas		Calculated Co^{2+} distribution		
Dehydrated zeolite		20000	(t+137000)/26.8	I	I'	% Co^{2+} on site I
$Co_{0.5}Y$						
	400°C	12425.1	2788.4	0.41	0.09	81.6
	500°C	14969.7	2575.4	0.43	0.07	86
$Co_{1.1}Y$						
	400°C	12836.1	3496.8	0.86	0.24	78
	500°C	13379.4	3385	0.88	0.22	80
$Co_{2.6}Y$						
	400°C	14311.5	6729.2	1.77	0.83	68
	500°C	22978.2	5200.9	2.12	0.48	81.5
$Co_{4.7}Y$						
	400°C	32786.4	8196.6	37.6	0.94	80
	500°C	31144.9	5447.8	4	0.7	85
$Co_{8.2}Y$						
	400°C	57095.9	9631	7	1.2	85
	500°C	40211	7963.5	6.8	1.4	83

t: triplet bands at 18700, 17100 and 15300 cm^{-1}.

3.4. Extra-lattice ligands

In all cases studied, the calcined Co^{2+} zeolites contain pseudo-tetrahedral species; i.e. an oxygen atom from residual H_2O molecules remains in the calcination sphere. This is not characteristic of Co^{2+} or transition metal ions in general. It has been reported for di-, tri- and tetravalent cations such as Ca^{2+}, La^{3+}, Ce^{3+} and Ce^{4+} [77–81]. The phenomenon becomes more important as the charge of the cation increases. Thus, $Ca(OH)^+$, $Ca_2(OH)_2^{2+}$, $[Ca–O–Ca]^{2+}$ species have been proposed on sites I' and II of faujasite-type zeolites [77]. But when the calcination temperature is increased to 700°C, the population of site I increases at the expense of the above-mentioned species. In the case of La^{3+}, Ce^{3+} and Ce^{4+}, the interaction with the zeolite is stronger [78–81]. Besides coordination of a residual water molecule, some lattice destruction might occur, giving extra-lattice Al and one or more oxygens in the coordination sphere might come from the lattice itself. In conclusion, it is possible to make a general scale of cation interaction, which is given in Table 4.

4. Cobalt in framework positions

Cobalt can be incorporated into the framework of AlPO-*n* structures [82–84]. The different

Table 4
Occurrence of an extra-lattice oxygen in the coordination sphere and of lattice destruction as a function of the charge of cations, exchanged in zeolites [73,74,77–81]

	Monovalent	Divalent	Trivalent	Multivalent
Extra-lattice oxygen	–	+	+	+
Lattice destruction	–	–	+	++

CoAPO-*n* structures are -5, -11, -14, -15, -16, -18, -20, -25, -34, -35, -36, -37, -39, -40, -41, -42, -44, -46, -47, -50 [39,40,85–111] and the CoAPSO structures are -34, -41, -44, -47 [88,100, 105,106,112–114]. It is assumed that Co^{2+} substitutes for Al^{3+}. Although cobalt is a suitable transition metal ion (TMI) to incorporate in a zeolite structure, because the ligand field stabilisation energies for Co^{2+} (d^7) disfavour the tetrahedral configuration relative to the octahedral one to a lesser extent than for most of the other d^n configurations, the Co content that can be incorporated in these alumino-phosphate structures is limited. Attempts to synthesize the AFI structure with high Co content usually lead to low-crystalline products contaminated with impurities [89]. The failure in obtaining a pure CoAPO-5 phase from Co-rich gels seems to be due to more favourable crystallization of other competing crystalline phases, such as the chabazite structure of CoAPO-34 [96,115]. Typical Co:Al ratios on CoAPO-*n* structures are given in Table 5. The highest Co:Al ratio reached in a CoAPO-*n* structure was 0.6, as is the case for CoAPO-50 [105]. Stucky recently developed zeolite analogue compounds based on cobalt phosphate with Co:Al>1 [116]. The highest cobalt incorporation is reached in his newly synthesized ACP-1 structure with Co:Al-8. The structure types [117] and Co:Al ratios are given in Table 5.

Table 5
Co:Al ratios for different types of cobalt-containing alumino-phosphate zeolites or zeolite analogue compounds

Structure type code	Co:Al = x	Reference
AFI (CoAPO-5)	0.06	[101]
AFY (CoAPO-50)	0.6	[105]
CHA (CoAPO-44)	0.25–0.3	[99,101,106]
CHA	>0.3	[116]
ANA	2	[116]
SOD	0.5, 3	[116]
GIS	x>0.33	[116]
MER	1.5<x≤3	[116]
PHI	3	[116]
ACP-1	8	[116]

The reported amounts of cobalt are not necessarily exclusively framework cobalt ions. When incorporating high amounts of Co^{2+}, some of the Co^{2+} can possibly be apparent as CoO or $CoAl_2O_3$ [64]. A directing factor during gel synthesis to stimulate incorporation of cobalt in the AFI structure is cooling the gel at 273 K [96]. Different criteria have been established for substitution of Co^{2+} for Al^{3+}: (1) a linear relation between intensity of bands of tetrahedral Co^{2+} with the amount of Co^{2+} in the samples; (2) a molar chemical composition Co+Al=P; (3) determination of IR bands of compensating protons (in the absence of charge-compensating template molecules); (4) a comparable volume of intrachannel void space of CoAPO-*n* and the corresponding AlPO-*n* (generation of extra-framework species would reduce the volume of intrachannel void space).

4.1. Spectroscopy

Because most of the spectroscopic data in the literature deal with CoAPO-5, this structure was chosen for a detailed spectroscopic description. The DRS bands of CoAPO-5 are given in Table 1. The triplet bands for the blue, as-synthesized CoAPO-5 are typical of tetrahedral Co^{2+}. Calcination in O_2 creates a yellow–green colour and a completely new spectrum. The triplet decreases in intensity and intense bands arise around 25 200 and 31 500 cm^{-1} [85,88,90]. They are usually ascribed to Co^{3+}. The bands at 25 200 and 31 500 cm^{-1} are totally removed by a reductive treatment in H_2, CO, NO, methanol, acetone,

water and toluene [85,88,90,91,93,95,96,98]. Because triplet bands are still present, part of the Co^{2+} in CoAPO cannot be oxidized. Evidence for the oxidation of Co^{2+} is also found by EPR. A significantly reduced EPR signal in calcined CoAPO-5 was explained by a partial oxidation of Co^{2+} to the EPR invisible Co^{3+} [88,90]. Lee proved the oxidative abilities of CoAPO-5 and -11 with EPR by the formation of radicals in interaction with alkenes [118]. Kurshev et al. showed that the difference in the EPR signal between an as-synthesized CoAPO-5 (having Curie–Weiss behaviour) and calcined CoAPO-5 (showing non-Curie–Weiss behaviour) is only valid at very low temperatures around 4 K and disappears at 20 K [97]. The $2D$ value of $-13\,cm^{-1}$ of calcined CoAPO-5 was explained by distortion of tetrahedral Co^{2+} to dihedral symmetry resulting from the interaction of Co^{2+} with two O_2 molecules. However, the non-Curie–Weiss behaviour can also be explained in terms of Co^{3+} in tetrahedral symmetry and no interactions with O_2 need to be invoked to create a distortion of the tetrahedron. Also, Pereira et al. [119] and Berndt et al. [101] suggested distortion of framework Co^{2+} to be the cause of the change in colour. On the basis of TPR and TPO experiments Berndt concluded that only non-framework cobalt species are reduced [101].

Combined in situ XRD and Co K-edge EXAFS studies recorded both during calcination and reduction have revealed simultaneous changes in bond lengths and oxidation states of the local structure of Co in CoAPO-5, CoAPO-18, CoAPO-36 and CoAPSO-44 catalysts [40]. The structure parameters are given in Table 6. Whereas the as-prepared materials clearly contain high-spin Co^{2+} in regular four-coordinated sites, complex behaviour is observed for their calcined forms. Various Co–O bond distances and coordination numbers are found, especially in the case of CoAPO-18 and CoAPSO-44. For CoAPO-18, a model was proposed with three short and one long Co–O distances. Complete oxidation of Co^{2+} to Co^{3+} in CoAPO-18 is established, with the local coordination of the high-spin Co^{3+} being distorted. In contrast, incomplete oxidation of the Co^{2+} is observed for CoAPO-5 and CoAPO-36.

Table 6
Structural parameters obtained from the EXAFS analysis for as-prepared, calcined and reduced CoAPO-*n* structures. N is the coordination number, R is the Co–O distance (reprint from ref. [40])

	As-prepared		Calcined		Reduced	
	N	R (Å)	N	R (Å)	N	R (Å)
CoAPO-5 (gel)	6.2	2.08				
CoAlPO-5	3.9	1.94	3.6	1.92	3.9	1.94
CoAlPO-36	4.0	1.92	3.25	1.87	4.1	1.93
CoAlPO-18	3.8	1.93	2.6	1.82	3.6	1.90
CoAlPO-18[a]			3.0	1.82	3.0	1.90
			1.0	2.04	1.0	2.04
CoAPSO-44	3.8		2.8	1.85	3.6	1.93

[a] Results of the analysis based on the distorted model.
Error limits for N and R are $\pm 10\%$ and ± 0.02 Å, respectively.

Till now, there have been no unambiguous spectroscopic criteria for framework and extra-framework Co^{2+}. On the basis of a systematic study of Co^{2+} in CoAPO-5 [120], the following interpretation was made: tetrahedral Co^{2+} in the lattice (after reduction) is characterized by $\nu_2 = 5500\,cm^{-1}$ and $\nu_3 = 15\,150\,cm^{-1}$, tetrahedral extra-framework Co^{2+} in the channel system has $\nu_2 = 5500\,cm^{-1}$ and $\nu_3 = 16\,850\,cm^{-1}$, octahedral Co^{2+} in the channel system has $\nu_1 = 8100\,cm^{-1}$ and $\nu_3 = 19\,550\,cm^{-1}$. Tetrahedral Co^{2+} in the lattice of as-synthesized CoAPO-5 has $\nu_2 = 6700\,cm^{-1}$ and $\nu_3 = 17\,300\,cm^{-1}$.

The amount of framework cobalt could be determined (1) from the weight loss during calcination, associated with the burning of Et_3NH^+: $Et_3NH^+ + 11O_2 \rightarrow 6CO_2 + 8H_2O + NO_2$; it is assumed that for every Co^{2+} in the lattice one Et_3NH^+ is needed to compensate the negative charge of the lattice; (2) the ratio of the amount of incorporated Co^{2+} in CoAPO-5s corresponds to the ratio of the band intensities at $15\,150\,cm^{-1}$ in the DRS spectra (confirming the proposed hypothesis that the $15\,150\,cm^{-1}$ band corresponds to framework Co^{2+} in CoAPO-5).

4.2. *Local coordination geometry and chemistry of* Co^{2+}

In CoAPO-5, in the presence of H_2O and template molecules, a perfect Co^{2+} tetrahedron is

formed. When the channels are empty after calcination, the tetrahedron is distorted. A similar phenomenon is found for Al in dehydrated H-ZSM-5 [121]. A quadrupole broadening of the ^{27}Al resonance was found upon dehydration, which points towards a distortion of the AlO_4 tetrahedron. Upon dehydration of H-boralite, the highly symmetric BO_4 tetrahedron is severely distorted [122]. Quadrupole parameters derived from the ^{11}B NMR spectra suggested that the effective coordination of boron changes from four to three. The general trend is therefore that when Si^{4+} is substituted for Al^{3+} in siliceous microporous materials and Al^{3+} by Co^{2+} (or any other transition metal ion) in microporous alumino-phosphates, an ideal tetrahedral coordination geometry (MO_4, $M=Al^{3+}$, Co^{2+}...) is obtained as long as lattice relaxation can occur via the molecules in channels and cages. This relaxation mechanism cannot happen after calcination, and distortion of the tetrahedron must occur due to differences in Si–O, Al–O, Co^{2+}–O, Co^{3+}–O... distances. A second source of distortion is that bridging hydroxyl groups are present for charge neutrality reasons, resulting in $M(Ox)_3(OH)$. A longer bond is associated with the protonated oxygen, similarly as for the protonated oxygen of acid-bearing Al^{3+} sites in alumino-silicates [123–127].

The degree of oxidation of Co^{2+} to Co^{3+} to CoAPOs follows the sequence CoAPO-18 > CoAPO-36 > CoAPO-5. For CoAPO-18, complete oxidation was derived on the basis of the Co–O distances, determined with EXAFS. When Co^{3+}–O and Co^{2+}–O are respectively taken as 1.83 and 1.94 Å, any partial oxidation can be derived from the relationship:

$$xR(Co^{3+}\text{–}O)+(1-x)R(Co^{2+}\text{–}O)=R_{exp}$$

with x the degree of oxidation of Co^{2+} and R_{exp} the experimental Co–O distance [40]. With such a relation, the distortion of the tetrahedra is not taken into account, nor the formation of extra-framework (octahedral) Co^{2+}. Barrett et al. explained the resistance to oxidation in CoAPO-5 and CoAPO-36 in comparison with CoAPO-18 by a higher extent of dehydroxylation in the former materials, which causes the formation of oxygen vacancies. Such a vacancy in the coordination sphere stabilizes Co^{2+}, but it is not clear why this occurs. In any case, the sequence of oxidation ability, given above, follows the increase of pore size or the decrease of the density of the structure: 3.8 Å < 6.5 × 7.5 Å < 7.3 Å. Thus, oxidation is easier in a more dense structure or Co^{2+} is better stabilized in a more open structure. The degree of distortion cannot be distinguished from the degree of oxidation, but it is anticipated to follow the same trend.

The highest degree of incorporation in CoAPO-n materials is established for $n=50$ [105]. From Table 5, the degree of incorporation follows the sequence: CoAPO-50 (AFY) > CoAPO-44 (CHA) > CoAPO-5 (AFI). The corresponding density of the T-atoms is 12.5 < 14.6 < 17.5 T/1000 Å^3, respectively. The degree of incorporation also seems to be facilitated by an open structure. In general, one can say, on the basis of a limited number of data, that the degree of oxidation, distortion and incorporation is dependent on the framework type, and more specifically on the density of the structure.

5. Concluding remarks

Thus, after calcination, Co^{2+} at ion exchange sites of zeolites X and Y occurs in three coordination geometries: trigonal and pseudo-tetrahedral at sites I′ and II, and pseudo-octrahedral at site I. Co^{2+} in zeolite A can have trigonal or pseudo-tetrahedral symmetry at the six-ring site (site I). However, recent Monte Carlo calculations on cation siting have given an indication that the real coordination geometry of cations in hexagonal prisms is also trigonal [128,129]. This observation needs further investigation.

The interaction of exchangeable cations with the lattice and with residual water molecules strongly increases with the charge of cations. Thus, trivalent and more highly charged cations give local lattice destruction. This is not the case for the divalent cations, including transition metal ions such as Co^{2+}. However, one can expect local site distortions (e.g. six-rings). We have obtained evidence that this is indeed the case and that the phenome-

non strongly depends on the number of Al-tetrahedra forming the six-ring site.

The degree of substitution of Co^{2+} in the lattice, the local distortion of the tetrahedra, the stability of Co^{2+} in the lattice and its ability to oxidize to Co^{3+} depend on the structure type of the AlPOs. The general trend is: the denser the AlPO structure, the fewer Co^{2+} can be substituted, the more distorted are the tetrahedra, the lesser the stabilization of Co^{2+}, the more Co^{2+} can be oxidized to Co^{3+}.

Acknowledgement

A.A.V. acknowledges a doctoral research grant of the I.W.T. and B.M.W. a post-doctoral fellowship of the Fonds voor Wetenschappelijk Onderzoek-Vlaanderen (F.W.O.). This work was financially supported by the Geconcerteerde Onderzoeksactie (G.O.A.) of the Flemish Government.

References

[1] K.A. Windhorst, J.H. Lunsford, J. Am. Chem. Soc. 97 (1975) 1407.
[2] T. Iizuka, J.H. Lunsford, J. Am. Chem. Soc. 100 (1978) 6106.
[3] S.-E. Park, J.H. Lunsford, Inorg. Chem. 26 (1987) 1993.
[4] B. Kraushaar-Czarnetzki, W.G.M. Hoogervorst, W.H.J. Stork, in: J. Weitkamp, H.G. Karge, H. Pfeifer, W. Hölderick (Eds.), Zeolites and Related Microporous Materials: State of the Art 1994, Studies in Surface Science and Catalysis, vol. 84, Elsevier, Amsterdam.
[5] D.L. Vanoppen, D.E. De Vos, M.J. Genet, P.G. Rouxhet, P.A. Jacobs, Angew. Chem., Int. Ed. Engl. 34 (1995) 560.
[6] Y. Li, J.N. Armor, U.S. Patent 5,149,512 (1992).
[7] Y. Li, J. Battavio, J.N. Armor, J. Catal. 142 (1993) 561.
[8] Y. Li, T.L. Slager, J.N. Armor, J. Catal. 150 (1994) 388.
[9] F. Witzel, G.A. Sill, W.K. Hall, J. Catal. 149 (1994) 229.
[10] K. Klier, R.G. Herman, S. Hou, in: J. Weitkamp. H.G. Karge, H. Pfeifer, W. Hölderick (Eds.), Zeolites and Related Microporous Materials: State of the Art 1994, Studies in Surface Science and Catalysis, vol. 84, Elsevier, Amsterdam, 1994, p. 1507.
[11] A.D. Cowan, R. Dumpelmann, N.W. Cant, J. Catal. 151 (1995) 356.
[12] D.B. Lukyanov, G. Sill, J.L. d'Itri, W.K. Hall, J. Catal. 153 (1995) 265.
[13] D.B. Lukyanov, J.L. d'Itri, G. Sill, W.K. Hall, in: J.W. Hightower, W.N. Delgass, E. Iglesia, A.T. Bell (Eds.), 11th International Congress on Catalysis—40th Anniversary, Studies in Surface Science and Catalysis, vol. 101, Elsevier, Amsterdam, 1996, p. 651.
[14] B.J. Adelman, T. Beutel, G.-D. Lei, W.M.H. Sachtler, J. Catal. 158 (1996) 327.
[15] A.W. Aylor, L.J. Lobree, J.A. Reimer, A.T. Bell, in: J.W. Hightower, W.N. Delgass, E. Iglesia, A.T. Bell (Eds.), 11th International Congress on Catalysis—40th Anniversary, Studies in Surface Science and Catalysis, vol. 101, Elsevier, Amsterdam, 1996, p. 661.
[16] L.J. Lobree, A.W. Aylor, J.A. Reimer, A.T. Bell, J. Catal. 169 (1997) 188.
[17] C. Montes de Correa, A. Luz Villa de P., Proc. 15th North American Catal. Soc. Meeting, 1997, p. 134.
[18] Y.-F. Chang, J.G. McCarty, J. Catal. 165 (1997) 1.
[19] A. Maes, A. Cremers, J. Chem. Soc., Faraday Trans. I 70 (1974) 165.
[20] D. Brae, K. Seff, Zeolites 17 (1996) 444.
[21] D.E. De Vos, E.J.P. Feijen, R.A. Schoonheydt, P.A. Jacobs, J. Am. Chem. Soc. 116 (1994) 4746.
[22] A.B.P. Lever, Inorganic Electron Spectroscopy, Elsevier, Amsterdam, 2nd edn., 1984.
[23] G. Kortüm, Reflectance Spectroscopy: Principles, Methods and Applications, Springer-Verlag, Berlin, 1969.
[24] R. Kellerman, Diffuse reflectance and photoacoustic spectroscopies, in: W.N. Delgass, G.L. Haller, R. Kellerman, J.H. Lunsford (Eds.), Spectroscopy in Heterogeneous Catalysis, Academic Press, New York, 1979, p. 86.
[25] R.A. Schoonheydt, Diffuse reflectance spectroscopy, in: F. Delannay (Ed.), Characterization of Catalysts, Marcel Dekker, New York, 1984, p. 220.
[26] N.N. Greenwood, A. Earnshaw, Chemistry of the Elements, Pergamon Press, Oxford, 1984, p. 1290.
[27] R.G. Burns, Mineralogical Applications of Crystal Field Theory, Cambridge University Press, Cambridge, 2nd edn., 1993, p. 234.
[28] R. Pappalardo, D.L. Wood, R.C. Linares Jr., J. Chem. Phys. 35 (1961) 2041.
[29] B.J. Hathaway, C.E. Lewis, J. Chem. Soc. A (1969) 1183.
[30] R. Reisfeld, C.K. Jørgensen, Structure and Bonding 77 (1992) 207.
[31] F.A. Cotton, D.M.L. Goodgame, M. Goodgame, J. Am. Chem. Soc. 83 (1961) 4690.
[32] H.A. Weakliem, J. Chem. Phys. 36 (1962) 2117.
[33] D.L. Wood, J.P. Remeika, J. Chem. Phys. 46 (1967) 3595.
[34] R.P. Van Stapele, H.G. Beljers, P.F. Bongers, H. Zijlstra, J. Chem. Phys. 44 (1966) 3719.
[35] J.N. McElearney, S. Merchant, G.E. Shankle, R.L. Carlin, J. Chem. Phys. 66 (1977) 450.
[36] M.W. Makinen, L.C. Kuo, M.B. Yim, G.B. Wells, J.M. Fukuyama, J.E. Kim, J. Am. Chem. Soc. 107 (1985) 5245.
[37] F.E. Mabbs, D. Collison, Electron Paramagnetic Resonance of Transition Metal Compounds, Elsevier, Amsterdam, 1992.
[38] G.E. Brown, G.A. Parks, P.A., O'Day, Sorption at mineral–water interfaces: macroscopic and microscopic perspec-

tives in mineral surfaces, in: D.J. Vaughan, R.A.D. Pattrick (Eds.), Mineral Surfaces, The Mineralogical Society Series, Chapman & Hall, New York, 1995, p. 129.
[39] J.M. Thomas, G.N. Greaves, Science 265 (1994) 1675.
[40] P.A. Barrett, G. Sankar, C.R.A. Catlow, J.M. Thomas, J. Phys. Chem. 100 (1996) 8977.
[41] M.D. Wirt, I. Sagi, E. Chen, S.M. Frisbie, R. Lee, M.R. Chance, J. Am. Chem. Soc. 113 (1991) 5299.
[42] M. Langlet, R. Guillamet, J. Durr, D. Gryffroy, R.E. Vandenberghe, Solid State Commun. 74 (1990) 1035.
[43] A. Jentys, N.H. Pham, H. Vinek, M. English, J.A. Lercher, Microporous Mater. 6 (1996) 13.
[44] Handbook of X-ray Photoelectron Spectroscopy, Perkin-Elmer Corp., 1992.
[45] T.L. Barr, Modern ESCA: The Principles and Practice of X-ray Photoelectron Spectroscopy, CRC Press, Boca Raton, FL, 1994.
[46] J.M. Stencil, V.U.S. Rao, J.R. Diehl, K.H. Rhee, A.G. Dhere, R.J. DeAngelis, J. Catal. 84 (1983) 109.
[47] G. Fierro, M.A. Eberhardt, M. Houalla, D.M. Hercules, W.K. Hall, J. Phys. Chem. 100 (1996) 8468.
[48] R.A. Schoonheydt, L.J. Vandamme, P.A. Jacobs, J.B. Uytterhoeven, J. Catal. 43 (1976) 292.
[49] W.-X. Zhang, H. Yahiro, M. Iwamoto, J. Izumi, J. Chem. Soc., Faraday Trans. 91 (4) (1995) 767.
[50] C.Y. Zhu, C.W. Lee, P.J. Chong, Zeolites 17 (1996) 483.
[51] C.W. Lee, P.J. Chong, Y.C. Lee, C.S. Chin, L. Kevan, Microporous Mater. 12 (1997) 21.
[52] D.B. Lukyanov, E.A. Lombardo, G.A. Sill, J.L. d'Itri, W.K. Hall, J. Catal. 163 (1996) 447.
[53] W.J. Mortier, Compilation of Extra Framework Sites in Zeolites, Butterworth, 1982.
[54] A.V. Boix, M.A. Ulla, J.O. Petunchi, J. Catal. 162 (1996) 239.
[55] H. Praliaud, G. Coudurier, J. Chem. Soc., Faraday Trans. I 75 (1979) 2601.
[56] K. Klier, in: H. Heineman (Ed.), Catalysis Review, Marcel Dekker, New York, 1968.
[57] K. Klier, J. Am. Chem. Soc. 91 (1969) 5392.
[58] P.F. Riley, K. Seff, J. Chem. Soc., Chem. Commun. (1972) 1287.
[59] T.A. Egerton, A. Hagan, F.S. Stone, J.C. Vickerman, J. Chem. Soc., Faraday Trans. I 68 (1972) 723.
[60] M.A. Heilbron, J.C. Vickerman, J. Catal. 33 (8) (1974) 434.
[61] H. Hoser, S. Krzyzanowski, F. Trifiro, J. Chem. Soc., Faraday Trans. I 71 (1975) 665.
[62] J.M. Jablonski, J. Mulak, W. Romanowski, J. Catal. 47 (1977) 147.
[63] P.J. Hutta, J.H. Lunsford, J. Chem. Phys. 66 (1977) 4716.
[64] J.H. Ashley, P.C.H. Mitchell, J. Chem. Soc. A (1968) 2861.
[65] K. Klier, P.J. Hutta, R. Kellerman, ACS Symp. Ser. 40 (1977) 108.
[66] K. Klier, Langmuir 4 (1988) 13.
[67] S. Wold, K. Esbensen, P. Geladi, Chemometrics and Intelligent Laboratory Systems 2 (1987) 37.
[68] P. Geladi, B.R. Kowalski, Anal. Chim. Acta 185 (1986) 1.
[69] D.M. Haaland, E.V. Thomas, Anal. Chem. 60 (1988) 1193.
[70] W. Windig, C.E. Heckler, F.A. Agblevor, R.J. Evans, Chemometrics and Intelligent Laboratory Systems 14 (1992) 195.
[71] W. Windig, D.A. Stephenson, Anal. Chem. 64 (1992) 2735.
[72] W. Windig, S. Markel, J. Mol. Struct. 292 (1993) 161.
[73] A.A. Verberckmoes, B.M. Weckhuysen, J. Pelgrims, R.A. Schoonheydt, J. Phys. Chem. 99 (1995) 15222.
[74] A.A. Verberckmoes, B.M. Weckhuysen, R.A. Schoonheydt, in: H. Chon, S.-K. Ihm, Y.S. Uh (Eds.), Progress in Zeolite and Microporous Materials, Studies in Surface Science and Catalysis, vol. 105, Elsevier, Amsterdam, 1997, p. 623.
[75] A.A. Verberckmoes, B.M. Weckhuysen, R.A. Schoonheydt, K. Ooms, I. Langhans, Anal. Chim. Acta 348 (1997) 267.
[76] P. Gallezot, B. Imelik, J. Phys. Chem. 71 (1974) 155.
[77] M.L. Costenoble, W.J. Mortier, J.B. Uytterhoeven, J. Chem. Soc., Faraday Trans. I 73 (1977) 466.
[78] M.L. Costenoble, W.J. Mortier, J.B. Uytterhoeven, J. Chem. Soc., Faraday Trans. I 74 (1978) 477.
[79] D.H. Olson, G.T. Kokotailo, J.F. Charnell, J. Colloid Interface Sci. 28 (1968) 305.
[80] P. Gallezot, B. Imelik, J. Chim. Phys. Physicochim. Biol. 68 (1971) 34.
[81] F.D. Hunter, J. Scherzer, J. Catal. 20 (1971) 246.
[82] S.T. Wilson, B.M. Lok, C.A. Messina, T.R. Cannan, E.M. Flanigen, J. Am. Chem. Soc. 104 (1982) 1146.
[83] E.M. Flanigen, R.L. Patton, S.T. Wilson, in: P.J. Grobet, W.J. Mortier, E.F. Vansant, G. Schulz-Ekloff (Eds.), Innovation in Zeolite Materials Science, Elsevier, New York, 1988, p. 13.
[84] J.A. Martens, P.A. Jacobs, in: J.C. Jansen, M. Stöcker, H.G. Karge, J. Weitkamp (Eds.), Advanced Zeolite Science and Applications, Studies in Surface Science and Catalysis, vol. 85, Elsevier, Amsterdam, 1994, p. 653.
[85] R.A. Schoonheydt, R. De Vos, J. Pelgrims, H. Leeman, in: P.A. Jacobs, R.A. Vansanten (Eds.), Zeolites: Facts, Figures, Future, Elsevier, Amsterdam, 1989, p. 559.
[86] N.J. Tapp, N.B. Milestone, L.J. Wright, J. Chem. Soc., Chem. Commun. (1985) 1801.
[87] N.J. Tapp, N.B. Milestone, D.M. Bibby, in: P.J. Grobet, W.J. Mortier, E.F. Vansant, G. Schulz-Ekloff (Eds.), Innovation in Zeolite Materials Science, Elsevier, Amsterdam, 1988, p. 393.
[88] L.E. Iton, I. Choi, J.A. Desjardins, V.A. Maroni, Zeolites 9 (1989) 535.
[89] V.P. Shiralkar, C.H. Saldarriaga, J.O. Perez, A. Clearfield, M. Chen, R.G. Anthony, J.A. Donohue, Zeolites 9 (1989) 474.
[90] C. Montes, M.E. Davis, B. Murray, M. Narayana, J. Phys. Chem. 94 (1990) 6425.
[91] B. Kraushaar-Czarnetzki, W.G.M. Hoogervorst, R.R.

Andréa, C.A. Emeis, W.H.J. Stork, J. Chem. Soc., Faraday Trans. 87 (6) (1991) 891.
[92] M.G. Uytterhoeven, W.A. Van Keyenberg, R.A. Schoonheydt, Mater. Res. Soc. Symp. Proc. 233 (1991) 57.
[93] M.P.J. Peeters, J.H.C. van Hoof, R.A. Sheldon, V.L. Zholobenko, L.M. Kustov, V.B. Kazansky, in: R. von Ballmoos et al. (Eds.), Proc. 9th Int. Zeolite Conf., Montreal, 1992, Butterworth-Heinemann, New York, p. 651.
[94] R. Roque-Malherbe, R. Lopez-Cordero, J.A. Gonzales-Morales, J. Oñate-Martinez, M. Carreras-Gracial, Zeolites 13 (1993) 481.
[95] J.W. Couves, G. Sankar, J.M. Thomas, J. Chen, C.R.A. Catlow, R. Xu, G.N. Greaves, in: R. von Ballmoos et al. (Eds.), Proc. 9th Int. Zeolite Conf., Montreal, 1992, Butterworth-Heinemann, New York, p. 627.
[96] M.G. Uytterhoeven, R.A. Schoonheydt, Microporous Mater. 3 (1994) 265.
[97] V. Kurshev, L. Kevan, D.J. Parillo, C. Pereira, G.T. Kokotailo, R.J. Gorte, J. Phys. Chem. 98 (1994) 10160.
[98] K. Nakashiro, Y. Ono, Bull. Chem. Soc. Jpn. 66 (1993) 9.
[99] J. Jänchen, M.P.J. Peeters, J.H.M.C. van Wolput, J.P. Wolthuizen, J.H.C. van Hoof, U. Lohse, J. Chem. Soc., Faraday Trans. 90 (7) (1994) 1033.
[100] U. Lohse, R. Bertram, K. Jancke, I. Kurzawski, B. Parlitz, E. Löffler, E. Schreier, J. Chem. Soc., Faraday Trans. 91 (7) (1995) 1163.
[101] H. Berndt, A. Martin, Y. Zhang, Microporous Mater. 6 (1996) 1.
[102] H.F.W.J. van Breukelen, G.J.C. Kraaijveld, L.J.M. van de Ven, J.W. de Haan, J.H.C. van Hooff, Microporous Mater. 12 (1997) 313.
[103] L. Marchese, J. Chen, J.M. Thomas, S. Coluccia, A. Zecchina, J. Phys. Chem. 98 (1994) 13350.
[104] C.V.A. Duke, S.J. Hill, C.D. Williams, Zeolites 15 (1995) 413.
[105] J.M. Bennett, B.K. Marcus, in: P.J. Grobet, W.J. Mortier, E.F. Vansant, G. Schulz-Ekloff (Eds.), Innovation in Zeolite Materials Science, Elsevier, New York, 1988, p. 269.
[106] S. Ashtekar, S.V.V. Chilukuri, A.M. Prakash, C.S. Harendranath, D.K. Chakrabarty, J. Phys. Chem. 99 (1995) 6937.
[107] A.M. Prakash, M. Hartmann, L. Kevan, J. Phys. Chem. B 101 (1997) 6819.
[108] D.B. Akolekar, J. Chem. Soc., Faraday Trans. 90 (7) (1994) 1041.
[109] S.J. Hill, C.D. Williams, C.V.A. Duke, Zeolites 17 (1996) 291.
[110] N. Rajic, A. Ristic, A. Tuel, V. Kaucic, Zeolites 18 (1997) 115.
[111] H.F.W.J. van Breukelen, Characterisation of CoAPO-5 and its application as catalyst for liquid phase oxidation reactions, Ph.D. Thesis, T.U. Eindhoven, 1998, p. 106.
[112] Y. Chu, P.J. Maddox, J.W. Couves, J. Chem. Soc., Faraday Trans. 86 (2) (1990) 425.
[113] J. Batista, V. Kaucic, N. Rajic, D. Stojakovic, Zeolites 12 (1992) 925.
[114] S. Hocevar, J. Batista, V. Kaucic, J. Catal. 139 (1993) 351.
[115] C. Urbina de Navarro, F. Machado, M. López, D. Maspero, J. Perez-Pariente, Zeolites 15 (1995) 157.
[116] P. Feng, X. Bu, G.D. Stucky, Nature 388 (1997) 735.
[117] W.M. Meier, D.H. Olson, Ch. Baerlocher, Atlas of Zeolite Structure Types, Elsevier, Amsterdam, 4th edn., 1996.
[118] Y.-J. Lee, H. Chon, J. Chem. Soc., Faraday Trans. 92 (18) (1996) 3453.
[119] C. Pereira, D.J. Parillo, G.T. Kokotailo, R.J. Gorte, in: J.B. Higgins, R. von Ballmoos, M.M.J. Treacy (Eds.), 9th Int. Zeolite Conf., Montreal, 1992, Extended Abstracts, p. 125.
[120] A.A. Verberckmoes, M.G. Uytterhoeven, R.A. Schoonheydt, Zeolites 19 (1997) 180.
[121] A.P.M. Kentgens, K.F.M.G.J. Scholle, W.S. Veeman, J. Phys. Chem. 87 (1983) 4357.
[122] K.F.M.G.J. Scholle, W.S. Veeman, Zeolites 5 (1985) 118.
[123] K.-P. Schröder, J. Sauer, M. Leslie, C.R.A. Catlow, J.M. Thomas, Chem. Phys. Lett. 188 (1992) 320.
[124] K.-P. Schröder, J. Sauer, M. Leslie, C.R.A. Catlow, Zeolites 12 (1992) 20.
[125] D.W. Lewis, C.R.A. Catlow, G. Sankar, S.W. Carr, J. Phys. Chem. 99 (1995) 2377.
[126] J.D. Gale, A.K. Cheetham, Zeolites 2 (1992) 674.
[127] R.A. van Santen, G.J. Kramer, Chem. Rev. 95 (1995) 637.
[128] R. Heidler, G.O.A. Janssens, W.J. Mortier, R.A. Schoonheydt, J. Phys. Chem. 100 (1996) 19728.
[129] G. Engelhardt, Microporous Mater. 12 (1997) 369.